Numerical optimization on the geometrical factors of a subsonic air-air ejector

HU Jian, CAO Xiaxin, HE Haisha, MENG Zhaoming, and DING Ming[1]

1. College of Nuclear Science and Technology, Harbin Engineering University, Harbin, China (E-mail: dingming@hrbeu.edu.cn)

Abstract: The ejectors can increase fluid pressure without directly consuming mechanical energy. They are widely used in many fields such as vacuum systems, refrigeration systems, fuel cells, chemical industry, aerospace and even core cooling systems of nuclear power plants. Although the structure of the ejector is simple, its internal flow field is very complex. Most existing design theories use semi-empirical and semi-theoretical methods. The design results deviate from the optimal structure, and a complete ejector size cannot be designed. In this study，the computational fluid dynamics (CFD) software, STAR-CCM+, was employed to investigate the effects of the geometrical factors of subsonic air-air ejectors. The mesh profile with 65669 elements has been proven to be sufficient to represent the ejector flow field. To investigate the accuracy of the numerical model, the experimental results and numerical simulation results were compared, which were in good agreement. The geometrical factors, such as the position of the nozzle, the ratio of the mixing chamber section area to the nozzle outlet section area, the length to diameter ratio of the mixing chamber and the angle of the diffuser, were obtained by numerical simulation to maximize entrainment ratio. The numerical results show that the optimal position of the nozzle was 100 **mm**, the optimal ratio of the mixing chamber section area to the nozzle outlet section area was 35, the optimal length to diameter ratio of the mixing tube was 4 and the optimal angle of the diffuser was 4 degrees.

Keyword: CFD; subsonic; air-air ejectors; geometrical factors

1 Introduction

The ejector consists of a working nozzle, acceptor chamber, mixing chamber, and a diffuser. The ejectors have the ability to increase suction flow pressure without consuming mechanical energy. Due to its simple structure, high reliability, easy maintenance, and low cost, therefore, the ejectors have been widely used in the fields of energy and power, petrochemicals, metallurgy, light industry and textiles, construction, refrigeration, and industrial thermal engineering at home and abroad. Recently, ejectors have also been used as flow recirculation systems and core cooling devices for large-scale boiling water reactors in nuclear power plants to improve the safety and economy of the systems [1-2].

A patent provides a spent fuel pool passive cooling system using injection technology [3]. In accident conditions, the high pressure gas in the gas tank cools the spent fuel pool by sucking cool air through the ejector. The key to this system is how to add to the suction flow rate. Therefore, it is necessary to study the influence of various structural parameters on the ejector to improve the suction flow rate.

Research on ejectors has been over 60 years. Keenan and Neumann [4] firstly proposed 1D model to predict the performance of the constant area mixing ejector. Then, Keenan *et al.* [5] induced the concept of the constant pressure mixing ejector, which is widely accepted by researchers. Later, many scholars took further amendments based on Keenan *et al's* proposed model [6-8]. Maqsood A,[9] conducted experimental study of subsonic air–air bent exhaust ejectors. DVORAK Vaclav [10] studied experimentally of subsonic air-air ejector with various configurations of the mixing chamber and the diffuser.

Theory and experiment cannot provide sufficient information about the ejection process because of the complexity of flow in ejectors. Improvements in computational power and methods allowed scientists to better understand the flow phenomena. Some reports of numerical analysis for the supersonic ejector are researched [11-14]. However, there are few studies on numerical simulation of subsonic air-air ejectors. The mixing process of subsonic air-air

Received date: November 14, 2018
(Revised date: January 12, 2019)

ejectors needs to be studied. In addition, it is necessary to study the performance of ejectors for various structural parameters under subsonic conditions. Using the CFD computer software, STAR-CCM+, a single factor analysis method was used to numerically study the effect of nozzle position, the ratio of the mixing chamber section to the nozzle outlet section, the length to diameter ratio of the mixing chamber, and the diffuser angle on the ejector performance. Furthermore, the influence rules of each parameter and the corresponding optimal parameters are reported. The study in this paper is conducive to further understanding the working process and principle of the ejector, and provides guidance and reference for the design of such ejectors.

2 Numerical simulation method

2.1 Geometry model

Since the flow region is regular and symmetric and the 2D axisymmetric model is used instead of the 3D model. The subsonic ejector geometric model is shown in Fig.1. The design parameters, such as primary and secondary pressures, used to create the supersonic air ejector are shown in Table 1(the pressure in the text is the gauge pressure). The commercial CFD software package, STAR-CCM+, is adopted to simulate the global performance and mixing processes of the subsonic air-air ejector.

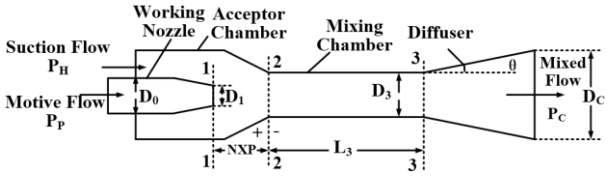

Fig.1 Subsonic air-air ejector geometry model.

Table 1 Design parameters of air ejector

Parameters	Symbols	Unit	Value
Primary pressure	P_P	Pa	60795
Secondary pressure	P_H	Pa	0
Discharged pressure	P_C	Pa	1084
Nozzle inlet diameter	D_0	mm	148
Nozzle outlet diameter	D_1	mm	44.2
Diameter of mixing tube	D_3	mm	301.6
Length of mixing tube	L_3	mm	2111.2
Angle of diffuser	θ	degree	4
Diffuser outlet diameter	D_C	mm	494
Nozzle exit position	NXP	mm	700

2.2 Two dimensional compressible conservation equations

The general form of conservation equations for compressible flow are given below:

Continuity equation:

$$\frac{\partial \rho}{\partial t}+\frac{\partial(\rho u_i)}{\partial x_i}=0 \tag{1}$$

Momentum equation:

$$\frac{\partial(\rho u_i)}{\partial x_i}+\frac{\partial(\rho u_i u_j)}{\partial t}=-\frac{\partial p}{\partial x}+\frac{\partial \tau_{ij}}{\partial x_j} \tag{2}$$

Energy equation:

$$\frac{\partial(\rho E)}{\partial t}+\frac{\partial(\rho u_i E+u_i p)}{\partial x_i}=\frac{\partial p}{\partial t}+\frac{\partial}{\partial x_i}(k_{eff}\frac{\partial T}{\partial x_i})+\frac{\partial}{\partial x_i}(u_i \tau_{ij}) \tag{3}$$

2.3 Physical model

The working fluid is air, density of the air is obtained using the ideal gas equation. Other properties are kept constant obtained from STAR-CCM data. The realizable k-ε two-layer model is employed to simulate the turbulent flow. The separation solver evolved from the classic SIMPLE algorithm was adopted, which is suitable for solving computational problems of incompressible flows and moderately compressible flows. The optional near wall treatment, all-y^+ wall treatment, was used in this study. The all-y^+ wall treatment is a kind of hybrid treatment. High-y^+ processing is attempted on the coarse grid, and low-y^+ processing is performed on the fine grid.

2.4 Boundary conditions

The motive flow inlet and the suction flow inlet were set as stagnation-inlet type. Meanwhile, the pressure-outlet type was applied to the mixed flow outlet. The total temperature of the motive flow inlet is 384 **K** and the total pressure is 60795 **Pa**. The total temperature of the suction flow inlet is 300 **K** and the total pressure is 0 **Pa**. The static pressure of mixed flow outlet is 1084 **Pa**. All the wall surfaces are set to be adiabatic since the heat loss at wall surfaces has less impact on the solution.

2.5 Convergence criteria

During the simulation, two converging criteria are adopted to obtain the converged solution: (1) The mass flow difference between the two inlet flows (motive flow and suction flow) and the outlet flow

(mixed flow) of the air ejector are no more than 10^{-6} **kg/s**. (2) All residual results are no larger than 10^{-5}.

2.6 Grid independent analysis

The subsonic air-air injector grid model as shown in Fig.2. The trimmer meshing model was adopted and performs different size encryption for areas with large velocity gradients or small size.

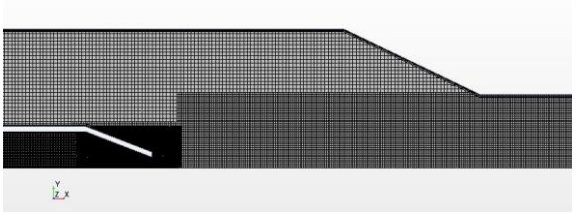

Fig.2 Meshes of subsonic air-air ejector.

In order to validating the accuracy of numerical solutions, the grid independent test has been performed for the physical model. Motive mass flow rate (G_P), suction mass flow rate (G_H) and mixed mass flow rate (G_C) are considered as the standards for the convergence of calculation. The entrainment ratio is defined as $u = G_H / G_P$. Four different numbers of grids were calculated. The changes of mass flow rate (G_P, G_H, G_C) and entrainment ratio u with the number of grids are shown in Figs.3 and 4.

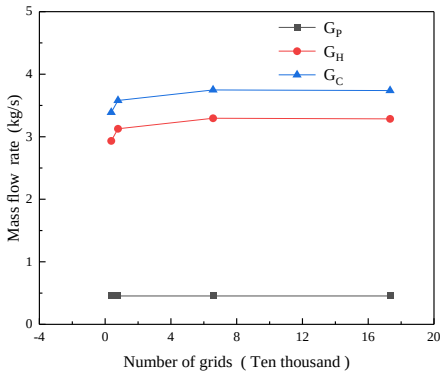

Fig.3 Mass flow rate changes with the number of grids.

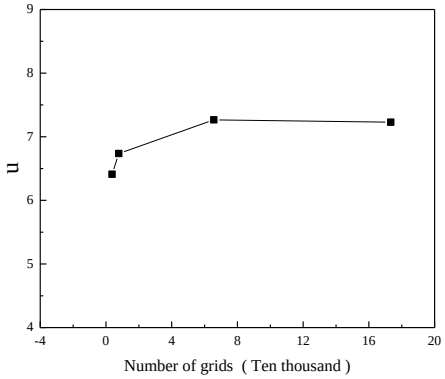

Fig.4 The u calculated by different grid number.

As shown in Figs.3 and 4, The changes of motive mass flow rate (G_P), suction mass flow rate (G_H), mixed mass flow rate (G_C) and entrainment ratio u between the calculated results of 65669 and 173382 mesh nodes are very small. Therefore, the gird system with 65669 mesh nodes is adopted for the following calculations.

2.7 CFD model validation

To illustrate the accuracy of CFD model, it is necessary to compare it with experimental or theoretical formulas. In the reference [11], an experimental study was conducted on the ejector. Numerical simulation of the ejector in the experiment was carried out in this paper. The research conditions in the experiment are as follows: the primary pressure P_P was 1.0 **MPa** and the secondary pressure P_H was 0.5 **MPa**. The range of discharged pressure was 0.4~0.7 **MPa**, and the studying of its influence on the entrainment ratio. The numerical simulation results were compared with experimental data, and it was shown in Fig.5. The experimental results are in good agreement with the numerical simulation results. Therefore, the numerical prediction in this paper has reasonable accuracy.

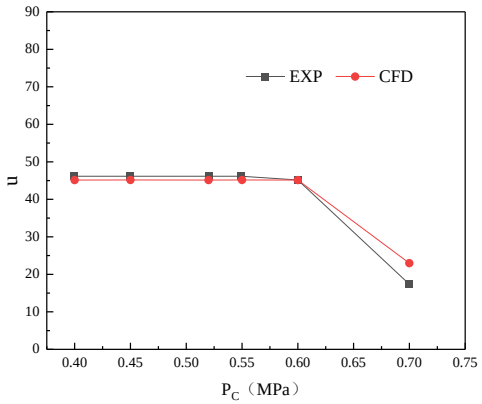

Fig.5 Comparison between numerical simulation results and experimental results.

3 Results and discussion

3.1 Flow field analysis

The velocity field distribution is shown in Fig.6 and the velocity is distributed along the axial direction as shown in Fig.7. From Figs.6 and 7, it can be seen that the velocity of the motive flow continues to increase after passing through the nozzle and reaches the maximum at the nozzle exit. At a distance from the nozzle, the axial velocity keeps the core maximum velocity constant. After the motive flow leaves the nozzle, it is continuously mixed with the suction flow, and the mixed boundary layer expands in stages. In the

mixing chamber, the motive flow and suction flow are further mixed, and the section velocity is continuously uniform. In the diffuser, the velocity of mixed flow becomes smaller due to the enlargement of the section.

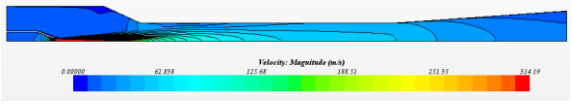

Fig.6 Velocity field.

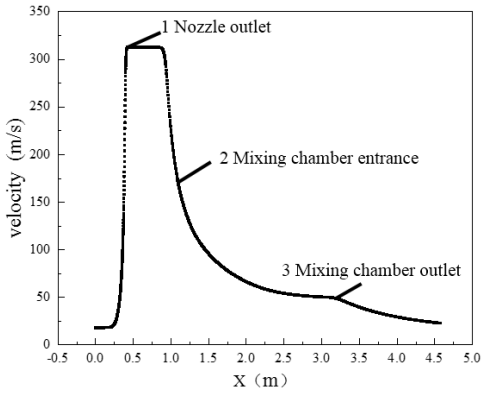

Fig.7 Axial velocity distribution.

The distribution of the pressure field is shown in Fig.8. The pressure field distributed along the axial direction as shown in Fig.9. It can be seen from Figs.8 and 9, after the high-pressure motive flow passes through the nozzle, the pressure drops sharply, a negative pressure is formed at the nozzle outlet, and the coil sucks fluid into the acceptor chamber. At a distance from the nozzle outlet, the axial pressure remains constant. The pressure is lowest at the inlet of the mixing chamber. In the mixing chamber, the motive flow and the suction flow are further mixed and the pressure is continuously increased. The pressure in the diffuser rises further due to the enlarged section area.

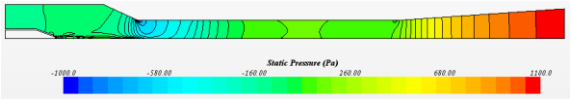

Fig.8 Pressure field.

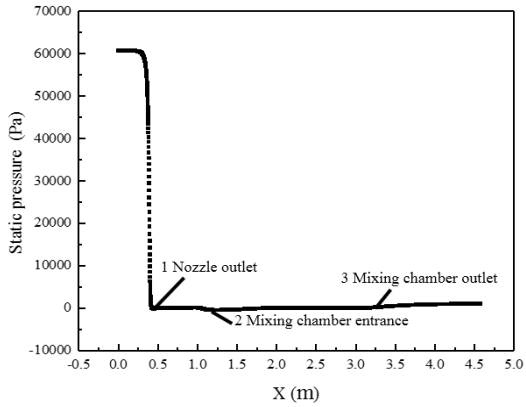

Fig.9 Axial pressure distribution.

3.2 Effect of structure parameter

3.2.1 Nozzle exit position

The entrainment ratio changes with nozzle exit position (NXP) which is one of the most important structure parameters is shown in Fig.10. NXP is defined as a positive value on the left side of the cylindrical mixing chamber. From Fig.10, it can be seen that as NXP changes from -400 to 1000 **mm**, the entrainment ratio increases first and then decreases. When NXP is in the range of 0-200 **mm**, the entrainment ratio is at a relatively large value .When the NXP is 100 **mm**, the entrainment ratio reaches a maximum of 9.21. The NXP is more or less than 100 **mm**, the entrainment ratio is smaller. The further the NXP deviates from 100 **mm**, the smaller the entrainment ratio.

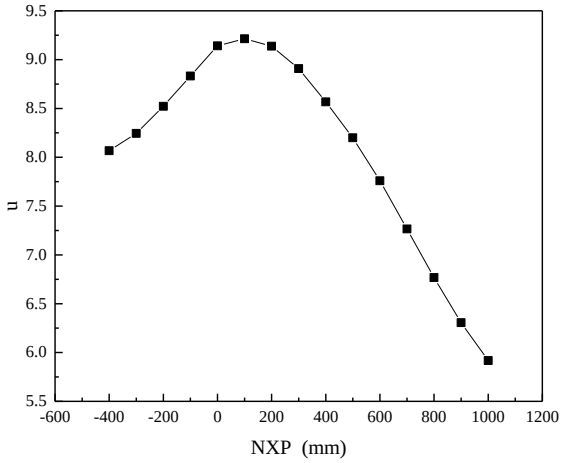

Fig.10 Variation of entrainment ratio with NXP

The axial static pressure distribution under different NXP is shown in Fig.11. It can be seen from Fig.11 that as the NXP changes from -400 to 1000 **mm**, the absolute value of the axial static pressure first increases and then decreases. The lower the negative pressure value of the axial static pressure, the greater pressure between suction flow

inlet and mixing chamber entrance, Which is beneficial to enhance the suction capacity. When NXP is 100 **mm**, the negative pressure reaches a minimum value of approximately -1500 **Pa**, which corresponds to the maximum entrainment ratio. With the increase of NXP, the lowest value of the axial static pressure continuously goes in the direction of the diffuser outlet.

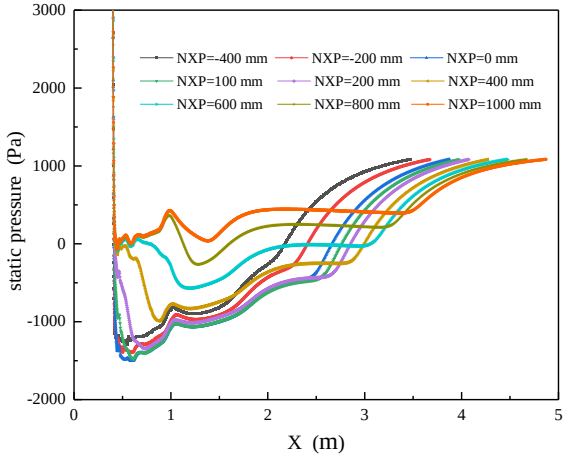

Fig.11 Axial static pressure distribution under different NXP.

3.2.2 Length to diameter ratio of the mixing chamber

The change of the entrainment ratio with the length to diameter ratio of the mixing chamber is shown in Fig.12, it can be seen that the length to diameter ratio of the mixing chamber changes from 2 to 10, the entrainment ratio increases first and then decreases. When the length to diameter ratio of the mixing chamber is 4, the entrainment ratio reaches a maximum of 7.65. When the length to diameter ratio is 3 to 5, the entrainment is relatively large. When the length to diameter ratio of the mixing chamber changes from 3 to 2, the entrainment ratio rapidly decreases.

The velocity radial distribution of the mixed gas at the outlet of the mixing chamber is shown in Fig.13, as the length to diameter ratio of the mixing chamber increases, the section velocity of the outlet of the mixing chamber is distributed uniformly in the radial direction.

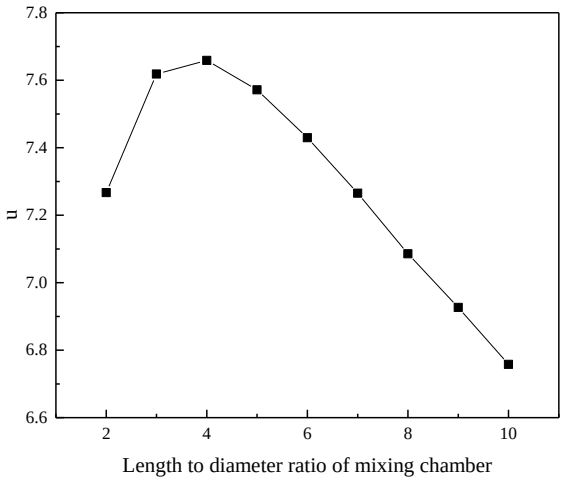

Fig.12 Variation of entrainment ratio with the length to diameter ratio of the mixing chamber.

The influence of the length to diameter ratio of the mixing chamber can be understood from two aspects: (1) The larger the length to diameter ratio of the mixing chamber, the better the mixing effect of motive gas and suction gas, and the more uniform the outlet section velocity along the radial direction of the mixing chamber is. The better the mixing effect in the mixing chamber, helps to increase the entrainment ratio. (2) The greater the length to diameter ratio of the mixing chamber, the greater the friction loss in the mixing chamber, which is not conducive to the increase of the entrainment ratio.

When the length to diameter ratio increases from 2 to 4, radial velocity of section at the outlet of the mixing chamber is more evenly distributed in the radial direction, and the entrainment ratio increases continuously. When the length to diameter ratio is 4, radial velocity of section at the outlet of the mixing chamber is distributed substantially uniformly in the radial direction, and then the aspect ratio is further increased, and the friction loss is continuously increased, resulting in a smaller entrainment ratio.

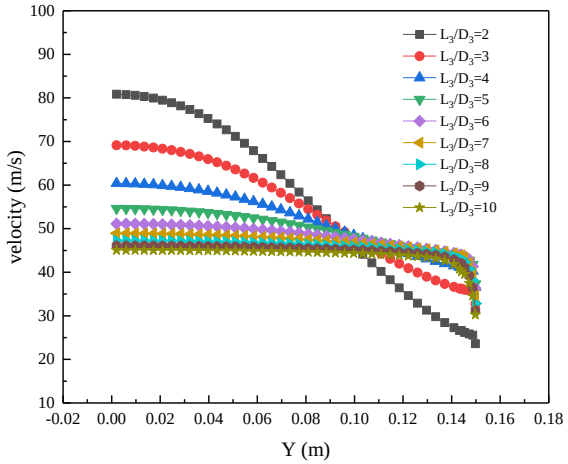

Fig.13 Radial distribution of velocity in mixing chamber outlet.

3.2.3 The ratio of the mixing chamber section area to the nozzle outlet section area

The entrainment ratio changes with the ratio of mixing chamber section area to the nozzle outlet section area is shown in Fig.14. It can be seen from Fig.14, the entrainment ratio approximately exhibits a parabolic distribution with the ratio of the mixing chamber section to the nozzle outlet section. When the ratio of the mixing chamber section area to the nozzle outlet section area changes from 15 to 65, the entrainment ratio increases first and then decreases. When the ratio of the mixing chamber section to the nozzle outlet section was 35, the entrainment ratio reached a maximum of 7.89.

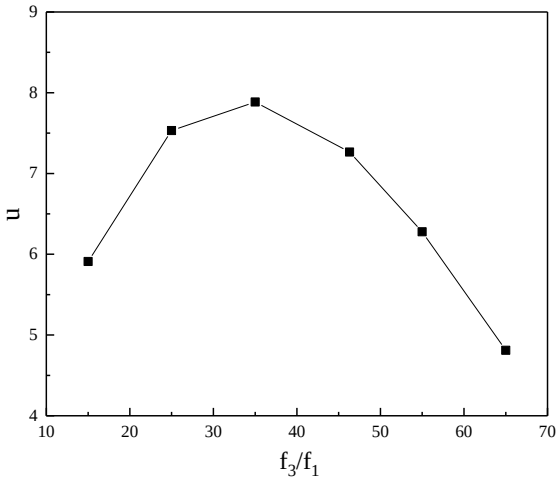

Fig.14 Variation of entrainment ratio with the ratio of the mixing chamber section area to the nozzle outlet section area.

The distribution of velocity fields at different ratio of the mixing chamber section area to the nozzle outlet section area is shown in Fig.15. According to the theory of literature [15], the closer the free jet final section to the inlet section of the mixing chamber, the better the ejector performance. It can be seen from Fig.15, the motive flow continues to mix with the suction flow after leaving the nozzle, and the mixing boundary layer continues to increase. When the ratio of the mixing chamber section area to the nozzle outlet section area is 35, the final cross section of the free jet is substantially equal to the inlet cross section of the mixing chamber, and the entrainment ratio reaches the maximum.

When the ratio of the mixing chamber section area to the nozzle outlet section area is less than 35, the final section of the free jet is larger than the inlet section of the mixing chamber, resulting in a large velocity gradient at the inlet of the mixing chamber, which is disadvantageous to the sucking of fluid and the entrainment ratio becomes smaller. When the ratio of the mixing chamber section area to the nozzle outlet section area is greater than 35, the flow velocity of the mixed flow near the wall surface of the mixing chamber is very slow, which is unfavorable to the mixing of the fluid and leads to a drop in the entrainment ratio.

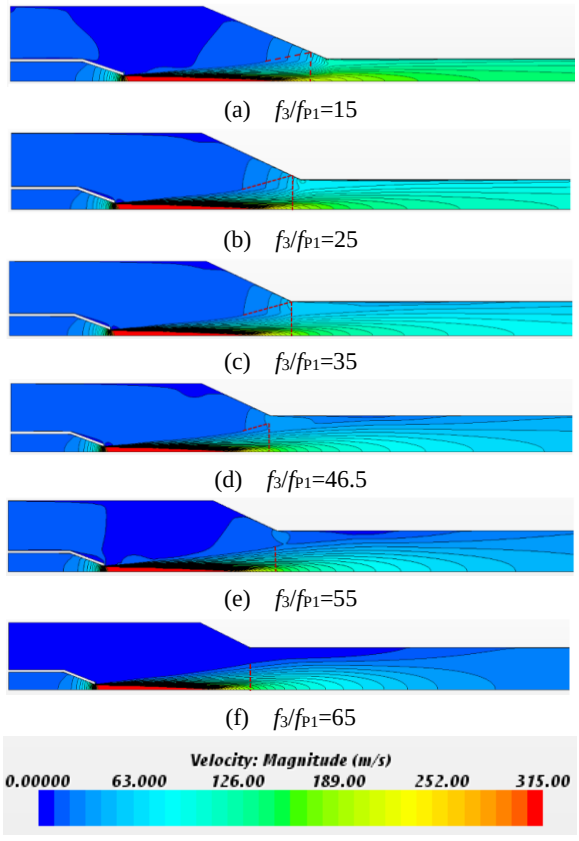

Fig.15 Velocity field distribution.

3.2.4 Diffusion angle

The entrainment ratio changes with the diffusion angle as shown in Fig.16. It can be seen from Fig.16, as the diffusion angle increases, the entrainment ratio increases first and then decreases. When the diffusion angle is 4 degrees, the entrainment ratio reaches a maximum of 7.27. The farther the diffusion angle deviates from 4 degrees, the smaller the entrainment ratio.

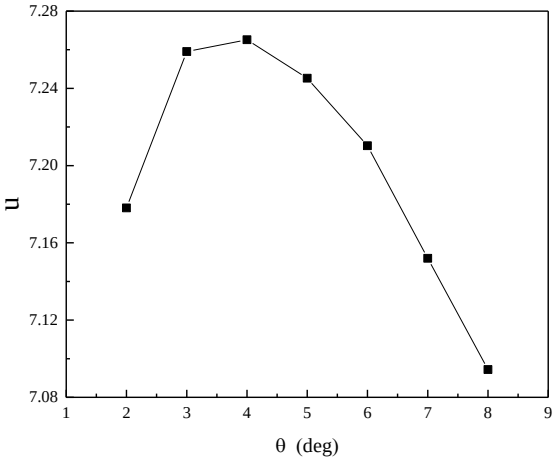

Fig.16 Variation of entrainment ratio with the diffusion angle.

The diffuser velocity field at different diffusion angles is shown in Fig.17. The influence of diffusion angle can be understood from two aspects: (1) The smaller the diffusion angle is, the longer the diffuser, and the more uniform the outlet section velocity of the diffusion section is along the radial direction, which is conducive to the increase of the entrainment ratio; (2) The smaller the diffusion angle is, the longer the diffuser, the greater the friction loss in the diffuser, which is detrimental to the increase of the entrainment ratio. It can be seen from Fig.17, the diffuser exit velocity is substantially uniform when the diffusion angle is 4 degrees. When the diffuser angle is less than 4 degrees, the diffuser exit velocity distribution does not change substantially but increases the diffuser friction loss. When the diffuser is greater than 4 degrees, the diffuser exit velocity is gradually non-uniform and the entrainment ratio decreases.

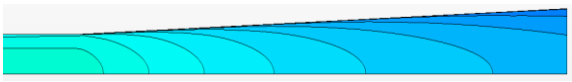

(a) $\theta = 2$ degree

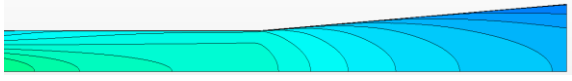

(b) $\theta = 4$ degree

(c) $\theta = 6$ degree

(d) $\theta = 8$ degree

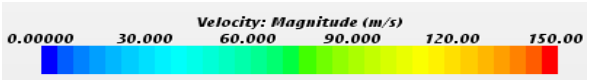

Fig.17 Diffuser velocity field distribution.

4 Conclusions

In this paper, the geometrical factors of an air-air ejector were investigated by the CFD technique, and the geometrical optimization presented contributed to significant improvement of the ejector performance. Based on the results of numerical simulation, the conclusions are summarized as follows:

(1) With the increase of NXP, the entrainment ratio increases first and then decreases. When the NXP belongs to 0~200 **mm**, the corresponding entrainment is relatively large. When the NXP is 100 **mm**, the entrainment ratio is a maximum of 9.21.

(2) As the length to diameter ratio of the mixing chamber increases, the entrainment ratio increases first and then decreases. When the length to diameter ratio of the mixing chamber is 3 to 5, the corresponding entrainment is relatively large. When the aspect ratio is 4, the entrainment ratio is a maximum of 7.65.

(3) The entrainment ratio approximately exhibits a parabolic distribution with the ratio of the mixing chamber section to the nozzle outlet section. At the ratio of the mixing chamber section area to the nozzle outlet section area of 35, the entrainment ratio is a maximum of 7.89. When the final section area of the jet at the outlet of the nozzle is equal to the inlet section area of the mixing chamber, the larger entrainment ratio is.

(4) As the diffusion angle increases, the entrainment ratio increases first and then decreases. When the diffusion angle is 4 degrees, the entrainment ratio is a maximum of 7.27. Compared to other geometric parameters, the diffusion angle has less influence on the entrainment ratio. In engineering applications, in order to reduce the injector size, the diffusion angle can be appropriately increased.

Nomenclature

d	——	diameter, mm
f	——	area, m^2
G	——	mass flow rate, kg/s
L	——	Length, mm
NXP	——	Nozzle exit position, mm
P	——	Pressure, Pa
T	——	Temperature, K
u	——	Entrainment ratio
θ	——	Diffusion angle, degree
Subscript		
0	——	Nozzle inlet section
1	——	Nozzle outlet section
2	——	Mixing chamber inlet section
3	——	Mixing chamber outlet section
C	——	Motive flow
H	——	Suction flow
P	——	Mixed flow

Acknowledgement

This paper is funded by Nuclear Safety and Simulation Technology Key Laboratory of National Defense Disciplines, Harbin Engineering University，the National Natural Science Foundation of China (No.11605033) and the Fundamental Research Funds for the Central Universities of Ministry of Education of China (Grant No. HEUCFJ181503).

References

[1] SUN, D. W., and EAMES, I. W.: Recent developments in the design theories and applications of ejectors [J]. Journal of the Institute of Energy, 1995, 68(475):65-79.

[2] LU, HX.: Jet Technology Theory and Application [M]. Wuhan University Press, 2004.

[3] DING, M., and HU, J., *et al.*: A High-Efficiency Passive Spent Fuel Tank Cooling System Using Jet Technology: CN107578828A [P]. 2018.

[4] KEENAN, JH., and NEUMANN, EP.: A simple air ejector. [J] Journal of Applied Mechanics. Trans ASME 1942; 64: A75-A81.

[5] KEENAN, J. H.: An Investigation of Ejector Design by Analysis and Experiment [J]. Journal of Applied Mechanics, 1950, 17(3):299-309.

[6] MUNDAY, J. T., and BAGSTER, D. F.: A New Ejector Theory Applied to Steam Jet Refrigeration [J]. Industrial & Engineering Chemistry Process Design & Development, 1977, 16(4):442-449.

[7] HUANG, B.J., CHANG, J.M., and WANG, C.P., *et al.*: A 1-D analysis of ejector performance [J]. International Journal of Refrigeration, 1999, 22(5):354-364. 111.

[8] ZHU, Y., CAI, W., and WEN, C., *et al.*: Shock circle model for ejector performance evaluation [J]. Energy Conversion & Management, 2007, 48(9):2533-2541.

[9] MAQSOOD, A.: A Study of Subsonic Air-Air Ejectors with Short Bent Mixing Tubes [J]. Dissertation Abstracts International, Volume: 69-03, Section: B, page: 1911. 2008.

[10] DVORAK, V.: Air to Air Ejector with Various Divergent Mixing Chambers [J]. Applied Mechanics & Materials, 2014, 493:50-55.

[11] CHONG, D., HU, M., and CHEN, W., *et al.*: Experimental and numerical analysis of supersonic air ejector [J]. Applied Energy, 2014, 130(sl):679-684.

[12] KRAC Ík, J., and DVOŘÁK, V.: Experimental and numerical investigation of an air to air supersonic ejector for propulsion of a small supersonic wind tunnel[C] 2015:02038.

[13] CHEN, W., CHEN, H., and SHI, C., *et al.*: A novel ejector with a bypass to enhance the performance [J]. Applied Thermal Engineering, 2016, 93:939-946.

[14] VAISHNAV, D., EHTESHAMI, M., and COLLINS, V., *et al.*: CFD Driven Parametric Design of Air-Air Jet Pump for Automotive Carbon Canister Purging [J]. 2017, 10(2).

[15] СОКОЛОВЕ, Я., and ЗИНГЕР, Н.: M.Ejector [M]. Huang Qiuyun, trans. Beijing: Science Press, 1977: 17-71.